Regulation of podocalyxin trafficking by Rab small GTPases in 2D and 3D epithelial cell cultures

Paulina S. Mrozowska and Mitsunori Fukuda

Laboratory of Membrane Trafficking Mechanisms, Department of Developmental Biology and Neurosciences, Graduate School of Life Sciences, Tohoku University, Sendai, Miyagi 980-8578, Japan

MDCK II cells, a widely used model of polarized epithelia, develop into different structures depending on culture conditions: two-dimensional (2D) monolayers when grown on synthetic supports or three-dimensional (3D) cysts when surrounded by an extracellular matrix. The establishment of epithelial polarity is accompanied by transcytosis of the apical marker podocalyxin from the outer plasma membrane to the newly formed apical domain, but its exact route and regulation remain poorly understood. Here, through comprehensive colocalization and knockdown screenings, we identified the Rab GTPases mediating podocalyxin transcytosis and showed that different sets of Rabs coordinate its transport during cell polarization in 2D and 3D structures. Moreover, we demonstrated that different Rab35 effectors regulate podocalyxin trafficking in 2D and 3D environments; trafficking is mediated by OCRL in 2D monolayers and ACAP2 in 3D cysts. Our results give substantial insight into regulation of the transcytosis of this apical marker and highlight differences between trafficking mechanisms in 2D and 3D cell cultures.

Introduction

Epithelial cells have a clearly defined apical–basolateral asymmetry, which is established through division of their plasma membrane into functionally and morphologically distinct domains. Apical and basolateral domains are comprised of distinct subsets of proteins and lipids, whose asymmetrical distribution is essential for epithelial cells to perform their physiological functions (Stoops and Caplan, 2014). So far, the most comprehensively characterized epithelial cell line is MDCK (Mardin–Darby canine kidney) II, and hence it is the most widely used in vitro model for studying mechanisms of polarization (Simmons, 1982). MDCK II cells create flat monolayers when grown on synthetic supports under traditional 2D culture conditions or spontaneously form 3D cysts when embedded in extracellular matrix analogs, such as Matrigel and collagen. Both of these structures share characteristic features of polarized epithelia with their surface divided into apical and basolateral domains. In contrast, a single epithelial cell has nonpolarized distribution of transmembrane proteins, i.e., they are spread evenly at the plasma membrane (Meder et al., 2005). During cell growth, proteins bound for different cellular domains undergo transcytosis from the outer plasma membrane to the newly formed apical or basolateral domain (Martin-Belmonte et al., 2007; Martin-Belmonte and Mostov, 2008). One of the proteins undergoing such transcytotic route, podocalyxin (PCX; also known as gp135), is a transmembrane glycoprotein localized exclusively to the apical domain and most often used as a marker in studies on the polarization of MDCK cells (Ojakian and Schwimmer, 1988). Because of extensive sialylation of its extracellular domain, PCX carries a highly negative charge that has been shown to be essential for maintaining the proper architecture of renal filtration apparatus (Kerjaschki et al., 1984; Doyonnas et al., 2001). Thus, delivery of PCX to the apical domain not only represents a hallmark of polarity establishment but also is crucial for building the morphology of renal epithelial tissue. Several regulators of PCX transcytosis have been identified so far; some of them are members of the Rab family of small GTPases. Rab GTPases are important coordinators of intracellular membrane trafficking and regulate various trafficking steps, including vesicle budding, uncoating, motility, docking, and fusion, through recruitment of specific effector proteins (Fukuda, 2008; Stenmark, 2009; Hutagalung and Novick, 2011). Four Rab family members (Rab3B, Rab8, Rab11A, and Rab27A) have been reported to mediate the final step of PCX transcytosis, i.e., docking of transport vesicles to the apical membrane (Bryant et al., 2010; Gálvez-Santisteban et al., 2012). However, regulators of steps other than the docking are yet to be identified, and thereby the exact route and molecular mechanism of PCX transcytosis remain poorly understood.

In this study, using a combination of colocalization and knockdown (KD) screenings, we performed a comprehensive analysis of Rab GTPase engagement in the transcytotic pathway of PCX during MDCK II polarization into 2D monolayers and 3D cysts and uncovered that the regulation of this pathway

Correspondence to Mitsunori Fukuda: nori@m.tohoku.ac.jp

Abbreviations used in this paper: KD, knockdown; KO, knockout; PCX, podocalyxin; RE, recycling endosome; TfR, transferrin receptor.

The Rockefeller University Press $30.00
J. Cell Biol. Vol. 213 No. 3 355–369
www.jcb.org/cgi/doi/10.1083/jcb.201512024

differs considerably between these two culture conditions. We further elucidated the mechanism of Rab35 engagement in PCX trafficking and demonstrated that under 2D and 3D culture conditions, Rab35 effectors are differently engaged in PCX trafficking, i.e., Rab35 works mainly with OCRL in 2D monolayers and with ACAP2 in 3D cysts. Our findings indicate that different sets of Rabs coordinately regulate PCX trafficking in 2D and 3D environments, even though PCX traverses the same organelles under both culture conditions (consecutively, early endosomes and Rab11-positive recycling endosomes) on its way to the apical membrane.

Results

PCX undergoes transcytosis in MDCK II cells growing under both 2D and 3D culture conditions

PCX is a highly glycosylated and sialylated protein that is specifically localized at the apical plasma membrane of polarized epithelial cells (Fig. S1, B and C). However, the exact route or mechanism of PCX trafficking to this site during polarity establishment is poorly understood. To determine the route of PCX trafficking in polarizing epithelial cells, we first generated a polyclonal antibody against the cytoplasmic domain of PCX and verified its specificity by siRNA treatment. The antibody specifically recognized a single band with an apparent molecular mass of 170 kD, and its signal mostly disappeared upon specific *PCX* siRNA treatment (Fig. S1 A, arrow). In addition, the same antibody was able to visualize endogenous PCX protein in an immunofluorescence analysis: signals of PCX were specifically observed at the apical plasma membrane of fully polarized MDCK II cells both under 2D and 3D culture conditions (Fig. S1, B and C). Moreover, siRNA-mediated KD revealed that PCX was not required for establishment of polarity, but its presence on the apical membrane was essential for epithelial morphogenesis (i.e., single-lumen formation) as described previously (Meder et al., 2005; Bryant et al., 2014). PCX-KD MDCK II cells showed normal E-cadherin staining pattern both in 2D and 3D cell cultures, but the monolayers appeared flattened (Fig. S1 B) and the lumen in cysts did not form properly (Fig. S1 C).

By using this specific antibody, we investigated the changes in subcellular localization of endogenous PCX protein on particular stages of MDCK II cell growth both under 2D and 3D culture conditions (Fig. 1). In brief, cells were seeded in low density, either on an uncoated glass-bottom dish (2D) or in Matrigel (3D), fixed in consecutive time points, and observed under a confocal fluorescence microscope. In 2D cell culture, PCX was initially evenly distributed on the plasma membrane. Upon contact with the glass-bottom dish, it was rapidly internalized and PCX-containing vesicles were directed to the compartment localized near the nucleus (1 h). Approximately 3 h after seeding, this PCX-positive compartment was translocated to the side under the nucleus. Intracellular localization of PCX was still visible at the two-cell and four-cell stage (16 and 24 h, respectively), but PCX vesicles were already undergoing exocytosis to the apical site, and 48 h after seeding, in fully polarized cells, PCX was present exclusively at the apical membrane (Fig. 1 A).

In 3D cysts growing in Matrigel, PCX showed similar trafficking pattern, although its internalization was slightly delayed, probably because of a different cue for transcytosis.12 h after seeding in Matrigel, PCX was still localized on the outer plasma membrane, but at the 16-h stage, it was present in the internal perinuclear compartment, the same as in 2D cell culture. Subsequently, PCX moved to the cell–cell contact site (24 h), where the apical domain was formed de novo and then the vesicles fused with the membrane where the lumen was created (72 h; Fig. 1 B). The comparison between PCX trafficking pattern in 2D and 3D cell cultures is summarized in schematic models shown in Fig. 1 C.

Previous studies have shown that during 3D cyst development, PCX is actively transcytosed (Martin-Belmonte et al., 2007; Martin-Belmonte and Mostov, 2008), whereas in 2D cell culture, it is constantly present at the apical membrane and does not undergo transcytosis (Meder et al., 2005). In contrast to these observations, our results showed that PCX is transported through the cytoplasm in both 2D (Fig. 1, A and C) and 3D cell cultures in a similar fashion (Fig. 1, B and C).

PCX is localized to parallel compartments in polarizing cells under both 2D and 3D culture conditions

Although PCX showed similar trafficking pattern in cells polarizing under both 2D and 3D culture conditions, it is not clear whether PCX is localized to the same intermediate compartments under both conditions. To determine that, we fixed MDCK II cells growing on a glass-bottom dish and in Matrigel at consecutive time points and costained the cells with antibodies against PCX and various organelle markers. PCX showed brief colocalization with an early endosome marker EEA1 both in 2D and 3D cell cultures at the early stages of cell growth (Figs. 2 A and S2 A). PCX did not colocalize with the Golgi marker GM130 in 2D or 3D cell culture (Figs. 2 B and S2 B), suggesting that observed intracellular PCX is not freshly biosynthesized but endocytosed. Intracellular signals of PCX were still observed even in the presence of cycloheximide, an inhibitor of protein synthesis (unpublished data). Because we expected transcytosed PCX to be localized to the recycling endosomes (REs), we also analyzed the colocalization with two RE markers: Rab11 and transferrin receptor (TfR). According to our previous data, Rab11 and TfR occupy different subpopulations of recycling endosomes, with TfR localized more to the outer fraction of REs and Rab11 to the inner fraction (Kobayashi and Fukuda, 2013b). In both 2D and 3D cell cultures, PCX colocalized extensively with Rab11 but showed only limited colocalization with TfR (Figs. 2 C and S2 C). Moreover, in terminally polarized cells under both conditions, Rab11 was similarly localized just below the apical membrane (Fig. 2 C), forming the so-called apical recycling endosome (Casanova et al., 1999), whereas TfR was scattered in the cytoplasm (Fig. S2 C). This interesting observation additionally revealed that in the process of polarity establishment in MDCK II cells, only the Rab11-positive inner fraction of REs transformed into the apical RE, whereas the TfR-positive outer fraction dispersed in the cytoplasm.

These observations indicate that in polarizing cells, endocytosed PCX rapidly traverses early endosomes and proceeds to Rab11-positive REs before being exocytosed to the apical membrane. A similar colocalization pattern with organelle markers in cells growing in both 2D and 3D cell cultures suggests the same trafficking pathway of PCX. Therefore, we decided to use 2D cell culture as a suitable model for studying the mechanism of PCX transcytosis during polarity development.

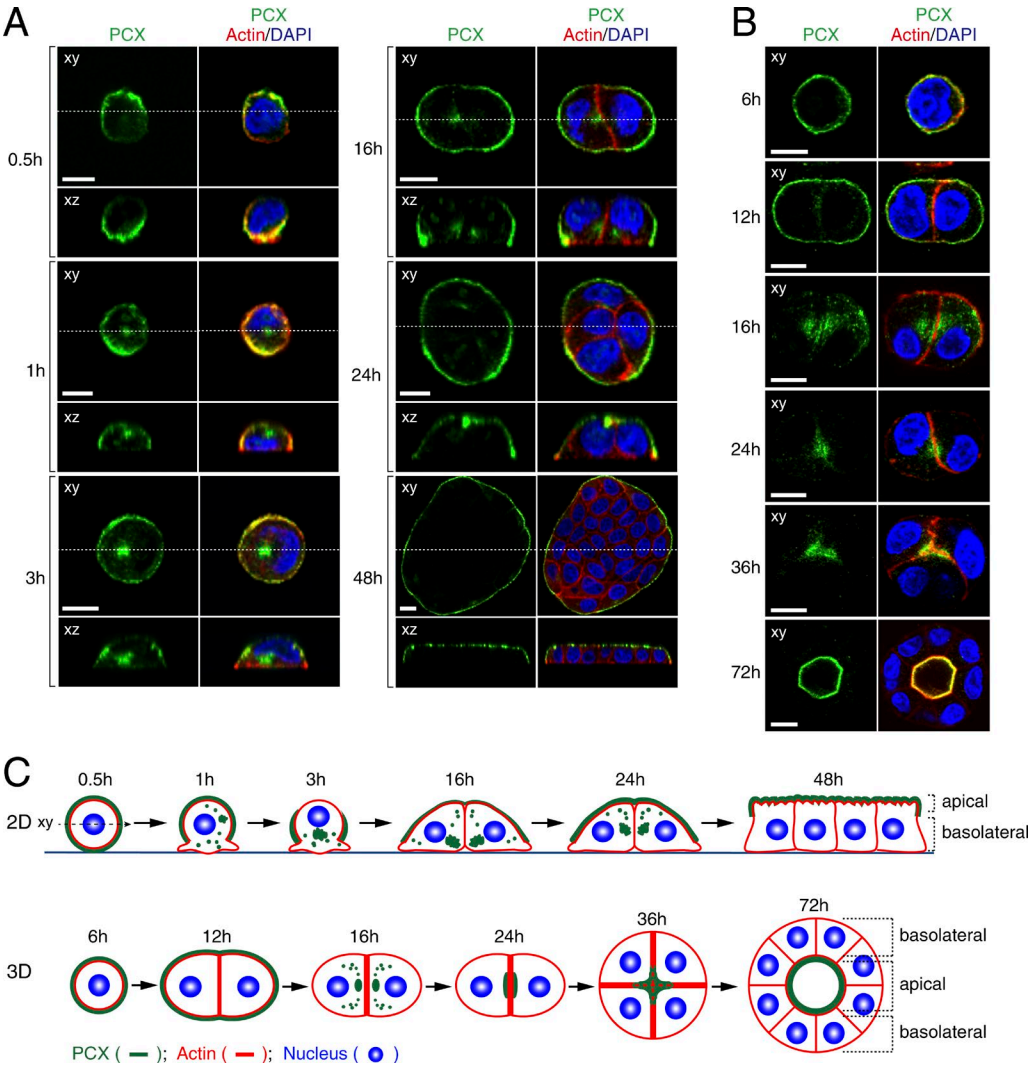

Figure 1. **Subcellular localization of endogenous PCX at consecutive time points in MDCK II cells growing in 2D monolayers and in 3D cysts.** (A and B) MDCK II cells were plated on glass-bottom dishes (A) or on Matrigel-coated glass slides (B) and fixed with PFA at the times indicated. The cells were then stained with anti-PCX antibody (green), Texas red–conjugated phalloidin (red), and DAPI (blue). The confocal xy section (top) and the xz section (bottom), which corresponds to the dashed line in the xy section, of 2D cell cultures are shown. Bars, 10 µm. The specificity of the anti-PCX antibody is shown in Fig. S1 A. (C) Schematic models presenting PCX localization during cell polarization into 2D monolayers (xz view; top) and 3D cysts (xy view; bottom). PCX is shown in green, actin in red, and the nucleus in blue.

Identification of candidate Rab GTPases engaged in PCX trafficking in 2D cell culture: colocalization screening and KD of colocalizing Rabs

Intracellular trafficking pathways are generally thought to be regulated by Rab small GTPases. So far, only four Rabs (Rab3B, Rab8, Rab11A, and Rab27A) are known to be engaged in PCX trafficking (Bryant et al., 2010; Gálvez-Santisteban et al., 2012), all of which mediate the docking of PCX vesicles to the apical membrane. However, nothing is known about the function of Rabs in other steps of PCX trafficking. To identify other Rab isoforms potentially involved in PCX trafficking, we performed a comprehensive colocalization screening between endogenous PCX and GFP (or Myc)-tagged Rab proteins. Because in 2D MDCK II cells PCX is transcytosed in the same manner as in 3D cells (Figs. 1 and 2), we used 2D cells in our initial colocalization screening, as they were easier to handle than Matrigel culture. We analyzed the colocalization of PCX with 60 different mammalian Rab GTPases at five consecutive time points (1, 3, 16, 24, and 48 h) representing different stages of PCX trafficking. The results of the screening are summarized in Table 1, Fig. 3, and Fig. S3.

The screening confirmed the colocalization of previously known regulators as well as revealed a subset of potentially new ones. Among the Rab GTPases that showed a high colocalization rate with PCX were regulators of endocytosis (Rab4, Rab5, and Rab35), transport from the TGN (Rab38) and intra-Golgi (Rab34), transport from REs to the plasma membrane (Rab3, Rab8, Rab10, Rab11, Rab23, Rab25, Rab27, and Rab33A), a tight junction regulator (Rab13), and others with less precisely specified function (Rab12 and Rab17; Hutagalung and Novick, 2011; Zhen and Stenmark, 2015). Because PCX is localized at REs, similarly to many Rab GTPases, a considerable amount of Rab proteins colocalized with PCX at this compartment. Fig. 3 shows colocalization pattern with RE-resident Rab17 as an example of a high colocalization rate and with Golgi-resident Rab36 as an example of poor colocalization. The results of the screening are schematically summarized in Fig. 3 C, and the full

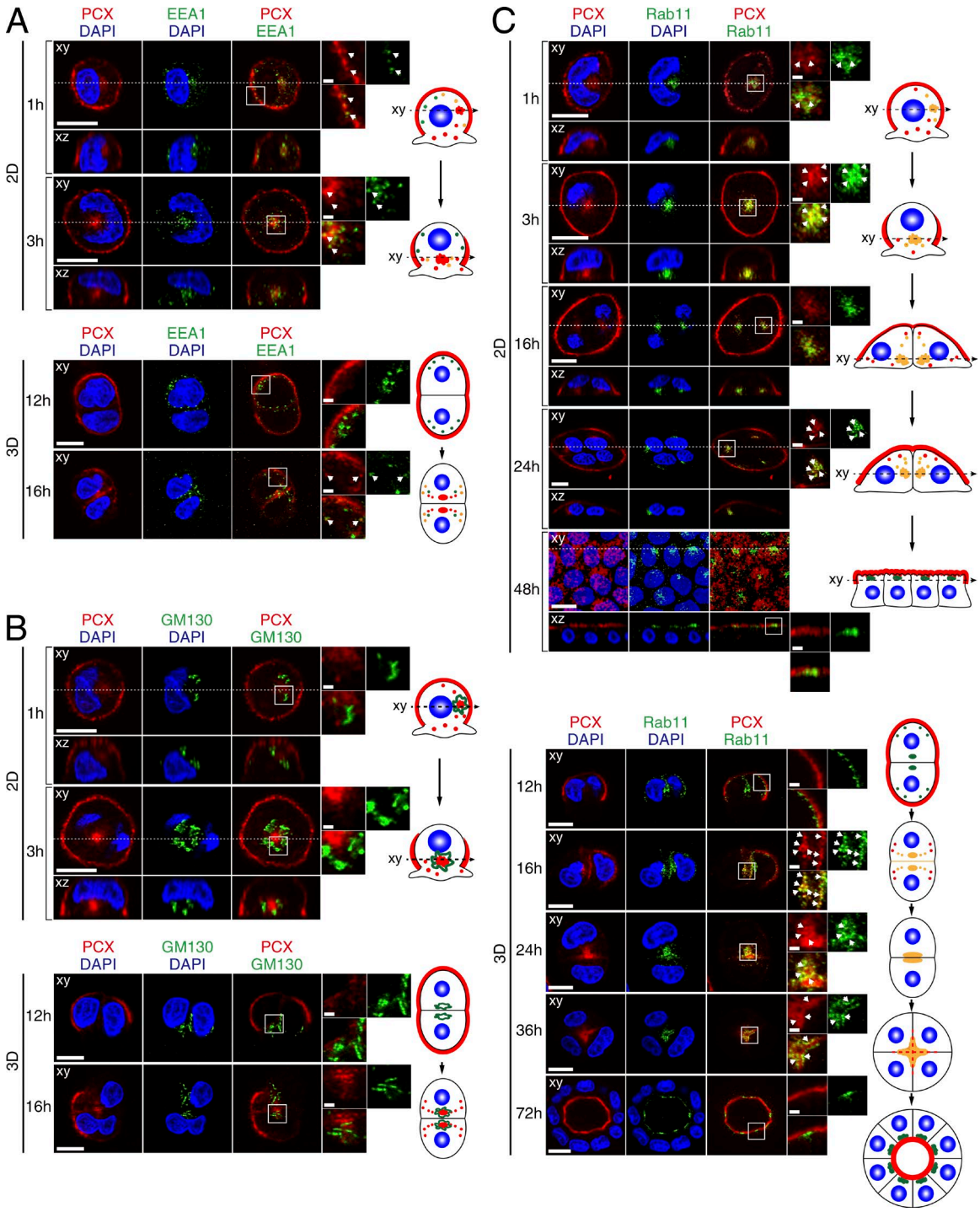

Figure 2. **PCX colocalization with organelle markers in 2D monolayers and in 3D cysts.** MDCK II cells were plated on glass bottom dishes (2D) or Matrigel-coated glass slides (3D) and fixed with PFA at the times indicated (see also Fig. S2). (A and B) Cells were costained with anti-PCX antibody (red), DAPI (blue) and an antibody against EEA1 (an early endosome marker; A), GM130 (a Golgi marker; B), or Rab11 (an RE marker; green; C). The confocal xy section (top) and the xz section (bottom), which corresponds to the dashed line in the xy section, of 2D monolayers are shown. The fourth columns show magnifications of the boxed regions in the third columns. The arrows in A show the colocalization points between EEA1 and PCX. Colocalization of PCX with each organelle marker is illustrated schematically on the right side of each panel (red, PCX; green, marker; yellow, colocalization site; and blue, nucleus). Bars: 10 µm; (insets) 1 µm.

microscopic images can be found in Fig. S3. However, because these results are obtained by expression of GFP-tagged Rabs, we cannot rule out possible artifacts resulted from overexpression.

To determine which of the Rab GTPases selected in the initial colocalization screening are effectively engaged in PCX trafficking, we subsequently analyzed the effect of their KD on PCX localization in 2D cell culture. Again, the localization of PCX was analyzed at five consecutive time points (1, 3, 16, 24, and 48 h) representing different stages of PCX trafficking. Rabs whose expression was not detected in MDCK II cells were

Table 1. **Summary of colocalization between endogenous PCX and Rabs in 2D MDCK II cells**

Rab	Time after plating				
	1 h	3 h	16 h	24 h	48 h
Rab1A	–	–	–	–	–
Rab1B	–	–	–	–	–
Rab2A	–	–	–	–	–
Rab2B	–	–	–	–	–
Rab3A	–	–	–	+/–	+/–
Rab3B	–	–	–	+	+/–
Rab3C	+/–	+/–	+	+	+/–
Rab3D	+/–	+/–	+	+	+/–
Rab4A	+/–	+/–	+/–	–	–
Rab4B	+/–	+/–	+/–	+/–	–
Rab5A	++	++	+	-	–
Rab5B	++	++	++	+	–
Rab5C	++	++	++	+	–
Rab6A	–	–	–	–	–
Rab6B	–	–	–	–	–
Rab6C	ND	ND	ND	ND	ND
Rab7	–	–	–	–	–
Rab8A	++	++	++	++	–
Rab8B	++	++	+	+/–	–
Rab9A	–	–	–	–	–
Rab9B	–	–	–	–	–
Rab10	+	+	++	+	–
Rab11A	++	++	++	++	+/–
Rab11B	++	++	++	++	+/–
Rab12	+	+	+/–	+/–	–
Rab13	+	+	–	–	–
Rab14	+/–	–	–	–	–
Rab15	+/–	+/–	+/–	–	–
Rab17	++	++	+	++	–
Rab18	–	–	–	–	–
Rab19	+	+	+/–	–	–
Rab20	+/–	+/–	+/–	–	–
Rab21	–	–	–	–	–
Rab22A	–	–	–	–	–
Rab22B	–	–	–	–	–
Rab23	+	+	–	–	–
Rab24	+/–	+	+	–	–
Rab25	+	+	++	+	+
Rab26	–	–	–	–	–
Rab27A	+	+	+	+	+
Rab27B	+	+	+	+	+
Rab28	–	–	–	–	–
Rab29	–	–	–	–	–
Rab30	–	+/–	+/–	–	–
Rab32	+/–	+	+/–	+/–	–
Rab33A	+/–	+	+	++	–
Rab33B	–	–	–	–	–
Rab34	+	+	+	+/–	–
Rab35	+	++	+/–	+	+/–
Rab36	–	–	–	–	–
Rab37	+/–	+/–	+/–	+/–	+/–
Rab38	+/–	+/–	+/–	+/–	–
Rab39A	–	–	–	–	–
Rab39B	–	–	–	–	–
Rab40A	ND	ND	ND	ND	ND
Rab40B	ND	ND	ND	ND	ND
Rab40C	–	–	–	–	–
Rab41	–	–	–	–	–
Rab42	–	–	–	–	–
Rab43	–	–	–	–	–

Colocalization rate between PCX and EGFP-Rabs (or Myc-Rab40C) in 2D MDCK II cells is shown by ++ (very high colocalization), + (partial but clear colocalization), +/– (partial and less colocalization), and – (no colocalization). ND, not determined because of very low expression level of Rab6C, Rab40A, and Rab40B in MDCK II cells. Detailed image data for each Rab are shown in Figs. 3 and S3. The nomenclature of mammalian Rabs in this study is as described in Itoh et al. (2008).

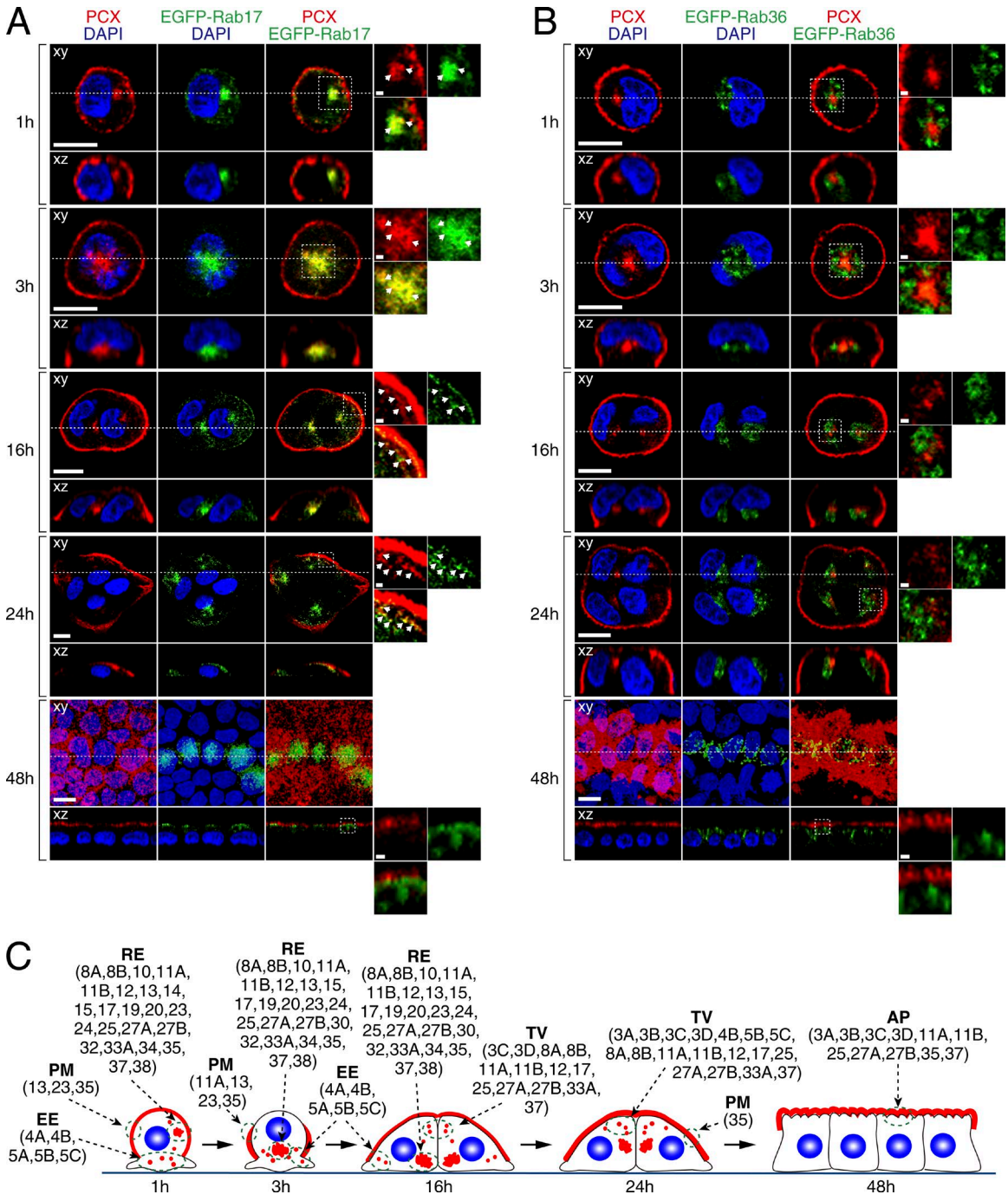

Figure 3. **Colocalization of endogenous PCX with EGFP-tagged Rab17 and Rab36 in 2D MDCK II cells.** MDCK II cells were transfected with plasmids carrying EGFP-tagged Rab17 (A) or Rab36 (B), plated on glass-bottom dishes, and fixed with PFA at the times indicated (see also Fig. S3). The cells were then stained with anti-PCX antibody (red) and DAPI (blue). The confocal xy section (top) and the xz section (bottom), which corresponds to the dashed line in the xy section, are shown. The fourth columns show magnifications of the boxed regions in the third columns. Bars: 10 µm; (insets) 1 µm. Note that EGFP-Rab17 and PCX were well colocalized at recycling endosomes just near the nucleus 1–3 h after plating and that their colocalization was also observed just beneath the plasma membrane (indicated by arrows) 24 h after plating. In contrast, no colocalization between EGFP-Rab36 and PCX was observed during PCX trafficking. (C) Schematic summary of the Rabs that colocalize with PCX (red) at specific membrane compartments (green doted circles) in 2D MDCK II cells (see also Table 1 and Fig. S3 for details). AP, apical plasma membrane; EE, early endosome; PM, plasma membrane; TV, transport vesicle.

omitted in the KD screening (Fig. S4 Y). Fig. 4 shows the comparison between control cells and different Rab-KD cells in the time points in which the most prominent morphological defect was observed. Generally, in 2D cell culture, KD phenotypes can be classified into eight groups: (1) PCX retention near cell–cell contact sites (Rab3 isoforms and Rab17), (2) lateral lumen formation (Rab5A, Rab5B, and Rab32), (3) intracellular retention of PCX (Rab8A, Rab13, and Rab27A), (4) delayed PCX vesicle docking without sustained intracellular retention (Rab11A), (5) increased cell spreading without visible PCX localization change (Rab15 and Rab19), (6) delayed PCX internalization (Rab14), (7) PCX retention in actin-rich clusters (Rab35), and

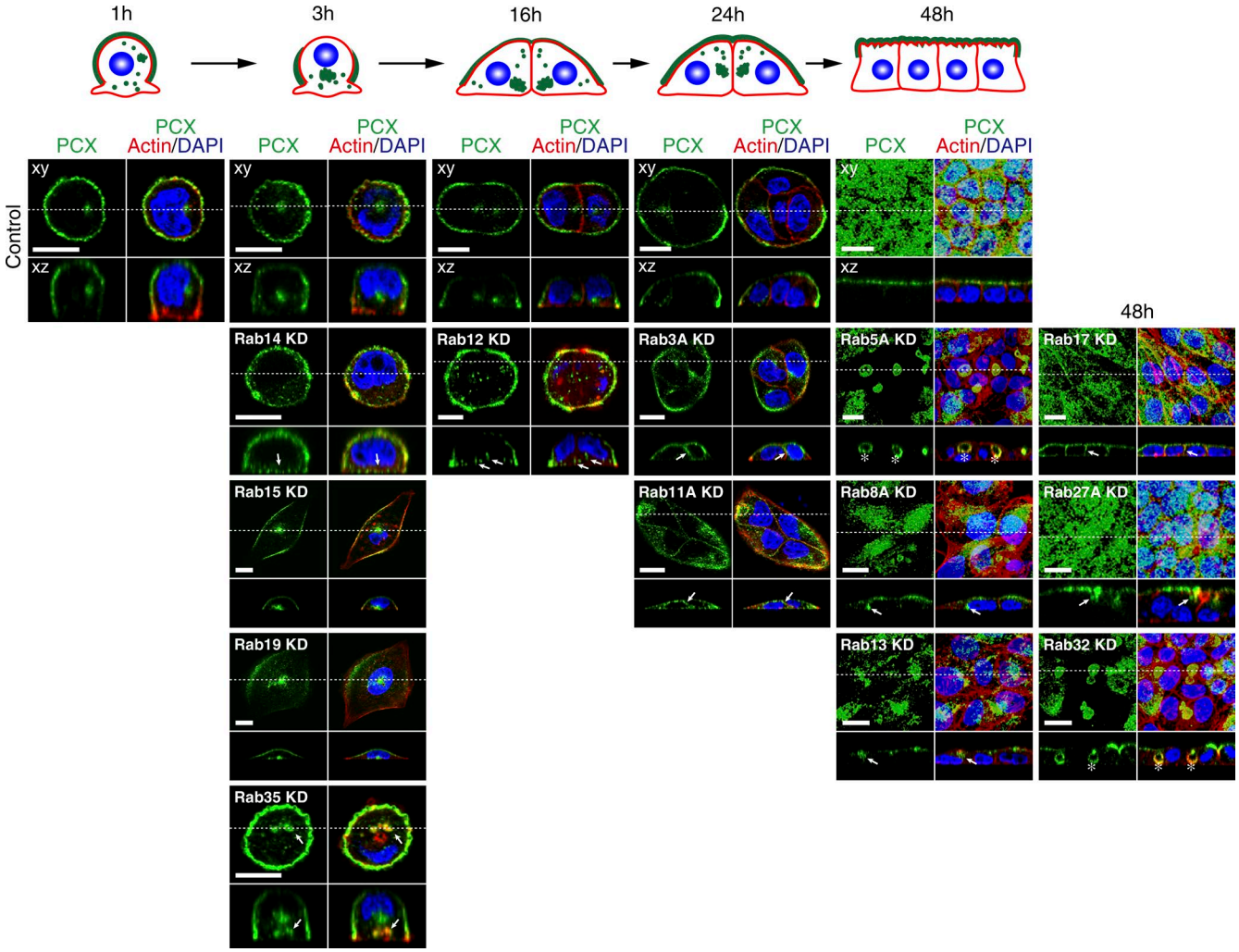

Figure 4. **Effect of KD of Rab GTPases on localization of endogenous PCX in 2D MDCK II cells.** MDCK II cells that had been treated with control siRNA (top row) or indicated *Rab* siRNA (other rows) were plated on glass-bottom dishes and fixed with PFA at the times indicated. The cells were then stained with anti-PCX antibody (green), Texas red–conjugated phalloidin (red), and DAPI (blue). The confocal xy section (upper) and the xz section (lower), which corresponds to the dashed line in the xy section, are shown. The localization of PCX in control cells is illustrated schematically above the microscopic images. The arrows point mislocalized PCX in comparison to the control cells. The asterisks indicate lateral lumens. Bars, 10 µm. The KD efficiency of siRNAs used and full images of Rab KD cells in all time points are shown in Fig. S4.

(8) PCX retention in multiple actin-free dots (Rab12; Fig. 4 and Table 2, middle column, Defects observed in 2D cell culture). Interestingly, although the suppression of aforementioned Rabs influenced the course of PCX trafficking at the early stages of polarization, depletion of only a subset of them impaired a proper apical localization of PCX in fully polarized cells (Table 2, right column, Defects in polarized 2D cells). Images showing the results of full KD screening can be found in Fig. S4.

KD of selected Rab GTPases potentially involved in PCX trafficking in 3D cysts

Because PCX is essential for lumen formation in developing cysts (Fig. S1 C), we assumed that any interference with PCX trafficking should disturb single-lumen formation. Because PCX is similarly transported to the apical membrane through early endosomes and Rab11-positive REs both under 2D and 3D culture conditions (Figs. 1 and 2), we hypothesized that Rabs, whose KD perturbed PCX trafficking in 2D cells (Fig. 4), also influence lumenogenesis. To test our hypothesis, we suppressed the expression of these Rabs in 3D Matrigel culture by specific siRNAs and observed the efficiency of single-lumen formation. The graph in Fig. 5 A shows the number of cysts with a single lumen for each depleted Rab, and the examples of the Rab-KD cysts and the full microscopic images of the Rab-KD cysts are presented in Fig. 5 and Fig. S5, respectively. The observed phenotypes can be roughly grouped as follows: (1) PCX retention near the newly formed apical site (Rab3 isoforms, Rab8A, Rab25, and Rab27A; Fig. S5), (2) PCX retention near the apical site and in scattered vesicles (Rab11A, Rab32, and Rab35; Figs. S5 and 5 B), (3) PCX retention in multiple large dots (Rab12; Figs. S5 and 5 B), (4) PCX retention in small intracellular vesicles without multiple lumen formation (Rab17; Fig. S5), (5) multiple lumens with PCX at the luminal membrane (Rab4A/B and Rab5A; Fig. S5), (6) reduced cyst proliferation (Rab5A and Rab24; Fig. S5 and not depicted; Table 2, left column, Defects observed in 3D cyst culture). Surprisingly, not all Rabs whose depletion influenced PCX trafficking in 2D cells also affected lumenogenesis in 3D cell culture (Fig. 5 C and Table 2). For example, KD of Rab13, which caused severe intracellular retention of PCX in 2D cells

(Fig. 4 and Fig. S4 L), did not affect PCX trafficking in 3D cysts, and they correctly formed single lumens with efficiency equal to the control cells (Fig. 5 A). Similarly, Rab14 KD, which in 2D cell culture inhibited PCX internalization (Fig. 4 and Fig. S4 M), had little effect on cyst formation (Fig. 5 A). In contrast, Rab25 KD, which had no effect on PCX trafficking in 2D cell culture (Fig. S4 T), markedly decreased single-lumen formation by blocking PCX localization at the apical membrane in 3D cysts (Fig. 5, A and B). KD of some Rabs also influenced PCX trafficking under both 2D and 3D culture conditions, but their KD phenotypes were strikingly different. The most prominent example was Rab35; Rab35 KD in 2D cells caused severe PCX entrapment in actin-rich structures (Fig. 4 and Fig. S4 X, arrows), whereas in 3D cysts, its KD led to PCX retention in large (sometimes weakly actin-positive) vesicles near the apical site (Fig. 5 B, arrows) and in multiple small actin-free vesicles in the cytoplasm (Fig. 5 B, arrowheads). Collectively, our Rab KD data from 2D and 3D cell cultures indicate that, even though PCX trafficking pathway appears to be the same under both conditions (Fig. 1 and Fig. 2), its regulation by Rab GTPases differs considerably between 2D monolayers and 3D cysts (Fig. 5 C and Table 2).

Rab35 regulates PCX trafficking through distinct Rab35 effectors under 2D and 3D culture conditions

To further investigate the differences in Rab35 involvement in PCX trafficking in 2D and 3D environments, we generated two independent Rab35-knockout (Rab35-KO) cell lines, named clone 18 (12-nt deletion) and clone 20 (1-nt insertion), by using the CRISPR/Cas9 system (Cong et al., 2013; Fig. 6, A and B). Clone 20 cells were plated on a glass-bottom dish and a Matrigel-covered glass slide and grown for 3 h and 24 h, respectively. PCX was stained with specific antibody and observed under a confocal fluorescence microscope. In 2D Rab35-KO cells, PCX was localized in clusters stained positively for actin (named "clustered PCX phenotype"; Fig. 6 C, arrowheads), the same as in Rab35-KD cells (Figs. 4 and Fig. S4 X). In 3D cysts, however, PCX stayed almost completely at the outer plasma membrane and the cysts failed to create lumens (Fig. 6 D), showing an "inverted phenotype" that was not observed in Rab35-KD cysts shown in Fig. 5 B. We noticed, however, that Rab35-KO cysts tended to revert back to normal polarity (with PCX localized at the centrally formed lumen, but not at the outer plasma membrane) with the culturing time, a tendency that was likewise observed for both Rab35-KO clones (Fig. 6 E). In Rab35-KO cysts, the transcytosis of PCX was delayed, but not completely stopped. The intracellular PCX en route to the newly formed apical site was most commonly observed 60–72 h after seeding (Fig. 6 E), in contrast to 16–36 h in control cysts (Fig. 1 B), presumably because of initial PCX retention at the outer plasma membrane. Because Rab35-KD cysts shown in Fig. 5 were grown for 72 h, a time after which the polarity of Rab35-KO cysts was almost completely reverted back to normal (Fig. 6 E), a long culturing time might have been the reason why we did not observe an inverted phenotype in Rab35-KD cysts. To investigate this possibility, we treated cells with siRNA against Rab35 and several other Rabs that most effectively decreased single-lumen formation in Fig. 5 A, and we observed their morphology 24 h after plating in Matrigel. As expected, almost 50% of Rab35-KD

Table 2. **Summary of impaired PCX localization in *Rab* siRNA-treated 2D and 3D MDCK II cells**

siRNA		Defects observed in 3D cyst culture		Defects observed in 2D cell culture	Defects in polarized 2D cells
Rab3A	+	Intracellular retention of PCX near the apical site	+/–	PCX retention near cell–cell contact sites	–
Rab3B	+	Intracellular retention of PCX near the apical site	+/–	PCX retention near cell–cell contact sites	–
Rab3D	+	Intracellular retention of PCX near the apical site	+/–	PCX retention near cell–cell contact sites	–
Rab4A/B	+/–	Some multiple lumens	–		–
Rab5A	+	Some multiple lumens; reduced proliferation	+	Lateral lumens	+
Rab5B	+	PCX retention in large actin-rich vacuoles	+	Lateral lumens	+
Rab5C	–		–		–
Rab8A	+	Intracellular retention of PCX near the apical site	+	Intracellular retention of PCX	+
Rab10	–		–		–
Rab11A	+	Intracellular retention of PCX near the apical site/ scattered vesicles	+	Delayed vesicle docking	–
Rab12	+	Retention of PCX in multiple large dots	+	Retention of PCX in multiple actin-free dots	–
Rab13	–		+	Intracellular retention of PCX	+
Rab14	–		+	Delayed vesicle internalization	–
Rab15	+	Intracellular retention of PCX	–	Increased spreading	–
Rab17	+	PCX retention in small intracellular vesicles	+	PCX retention near cell–cell contact sites	+
Rab19	+	Intracellular retention of PCX	–	Increased spreading	–
Rab20	–		–		–
Rab23	–		–		–
Rab24	–	Reduced proliferation	–		–
Rab25	+	Intracellular retention of PCX near the apical site	–		–
Rab27A	+	Intracellular retention of PCX near the apical site	+/–	Slight intracellular retention of PCX	+/–
Rab32	+	Intracellular retention of PCX near the apical site/ scattered vesicles	+	Lateral lumens	+
Rab34	–		–		–
Rab35	+	Intracellular retention of PCX near the apical site/ scattered vesicles	+	Intracellular retention of PCX in actin-rich clusters	+

Defects in PCX localization are shown by + (clear defect), +/– (mild defect), and – (no defect). Detailed image data are shown in Figs. 4, 5, S4, and S5.

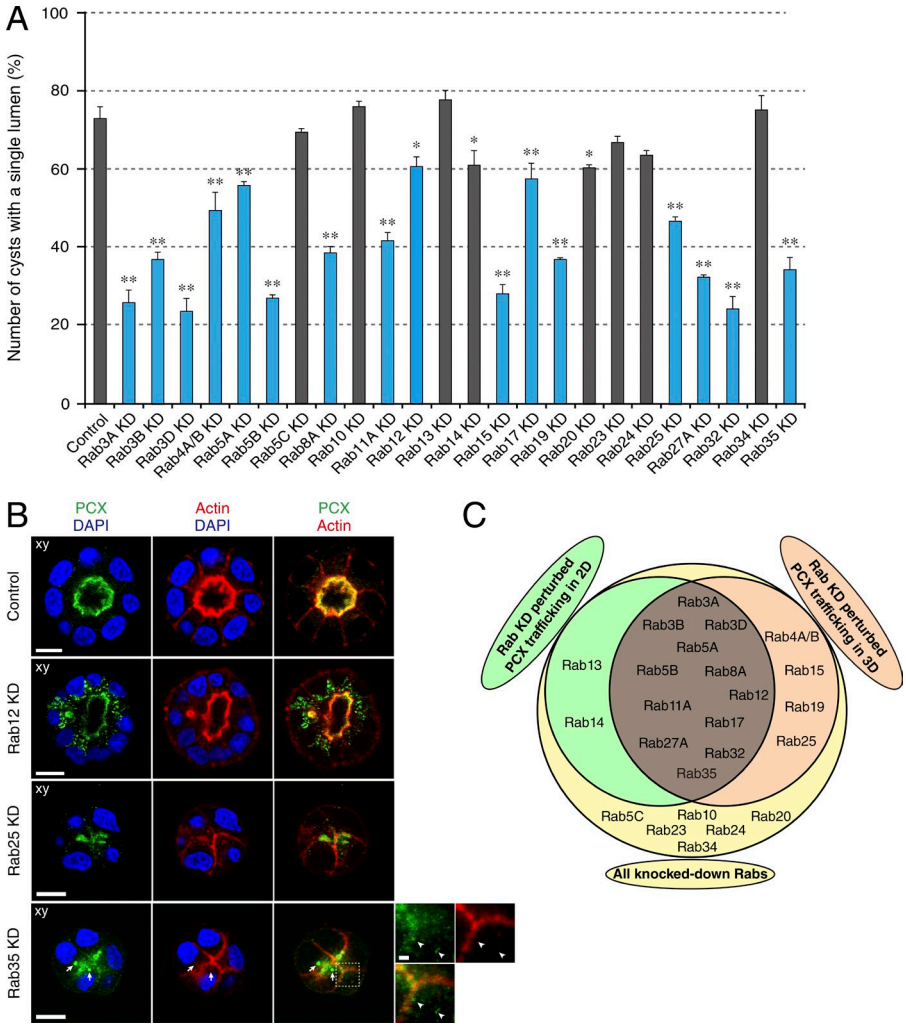

Figure 5. **Effect of KD of Rab GTPases on single-lumen formation in 3D MDCK II cells.** MDCK II cells that had been treated with control siRNA or indicated *Rab* siRNA, were plated on Matrigel-coated glass slides and fixed with PFA 72 h after plating. The cells were then stained with anti-PCX antibody (green), Texas red–conjugated phalloidin (red), and DAPI (blue). (A) Percentage of single-lumen formation in cysts treated with control siRNA or indicated *Rab* siRNA. Values represent the mean and SEM of at least three independent experiments ($n > 100$ in each experiment). We focused on Rabs whose KD caused reduction in single-lumen formation <60% (blue bars; indicated as + in Table 2). Although the rate of single-lumen formation of Rab12-KD cells exceeds 60%, they exhibited a different phenotype, i.e., PCX retention in multiple large dots (also shown as a blue bar; see also the second panel in B). Significance was determined by one-way analysis of variance with Dunnett's post-test at 95% confidence interval. *, $P < 0.05$; **, $P < 0.01$. (B) Representative microscopic images of cysts treated with the indicated *Rab* siRNA. Bars: 10 µm; (insets) 1 µm. The arrows point to large PCX vesicles near the apical membrane that are also weakly positive for actin. The arrowheads in the right insets show small actin-free PCX vesicles in the cytoplasm. (C) The graph grouping all KD Rabs (yellow circle), which influenced PCX trafficking in 2D cells (green circle) and 3D cysts (orange circle). Rabs in the green and orange overlap region influenced PCX trafficking both under 2D and 3D culture conditions, Rabs in the green-only region affected PCX trafficking only in 2D cell culture, Rabs in the orange-only region had an effect only in 3D culture, and Rabs in the yellow-only region had no effect on MDCK II cell morphology at all. The KD efficiency of siRNAs used is shown in Fig. S4. Images of all Rab KD cysts showing defects in single-lumen formation are shown in Fig. S5.

cysts, but not other Rab-KD cysts, retained PCX on the outer plasma membrane (Fig. 6 F), the same as Rab35-KO clones. A total of 84 h and 96 h after seeding, Rab35-KO cysts were fully developed and the PCX accumulation at the intracellular puncta, as observed in 72-h Rab35-KD cysts (Fig. 5 B), was no longer observed. Thus, the intracellular PCX accumulation observed in 72-h Rab35-KD cysts (Figs. 5 B and S5) is likely to be caused by its prolonged retention at the outer plasma membrane and delayed transcytosis and not by a defect in vesicular transport itself.

Rabs generally control membrane trafficking through interaction with their specific effector molecules (Fukuda, 2008; Zhen and Stenmark, 2015). To molecularly understand the difference in Rab35-depletion (clustered PCX phenotype in 2D cells versus inverted phenotype in 3D cysts), we attempted to identify effector molecules of Rab35, through which Rab35 regulates PCX trafficking in 2D and 3D cell cultures. So far, at least five different Rab35 effectors have been reported in mammals: ACAP2 (also known as centaurin-β2; Kanno et al., 2010; Kobayashi and Fukuda, 2012), Fascin (Zhang et al., 2009), MICAL1 (Fukuda et al., 2008), MICAL-L1 (Fukuda et al., 2008; Rahajeng et al., 2012; Kobayashi and Fukuda, 2013a), and OCRL (Fukuda et al., 2008; Dambournet et al., 2011). Because all five Rab35 effectors are endogenously expressed in MDCK II cells, we depleted each effector with specific siRNAs (Fig. 7 C), and the 2D and 3D KD cells were observed to determine PCX localization. Provided that certain Rab35 effector functions together with Rab35 during PCX trafficking in developing 2D monolayers or 3D cysts, its KD should phenocopy Rab35 deficiency. In 2D KD cells growing on glass-bottom dishes, the clustered PCX phenotype was mimicked largely by the suppression of OCRL and to the lesser extent by that of ACAP2 (Fig. 7 A). To further confirm the importance of Rab35–effector interaction during PCX trafficking, we used two recently developed Rab35 mutants with amino acid substitutions in the switch II effector region (Etoh and Fukuda, 2015): a Rab35(TS/TA) mutant with decreased binding affinity only for ACAP2 and a Rab35(S5A) with decreased affinity for all the effectors, including OCRL. In control cells, intracellular PCX showed extensive colocalization with the recycling endosome marker Rab11 (Fig. 2 C and Fig. 7 D, arrows, and Fig. 7 E), whereas in Rab35-KO cells, such colocalization was almost completely lost (Fig. 7, D and E) and instead PCX clusters were often colocalized with actin (Fig. 7 D, arrowheads). To determine the ability of Rab35 mutants to rescue the PCX trafficking defect, we quantified the Pearson's correlation coefficient of colocalization between PCX and Rab11 in Rab35-KO cells expressing Rab35 mutants. The reexpression of Rab35 wild type in Rab35-KO cells was able to completely rescue the colocalization and, to a considerable

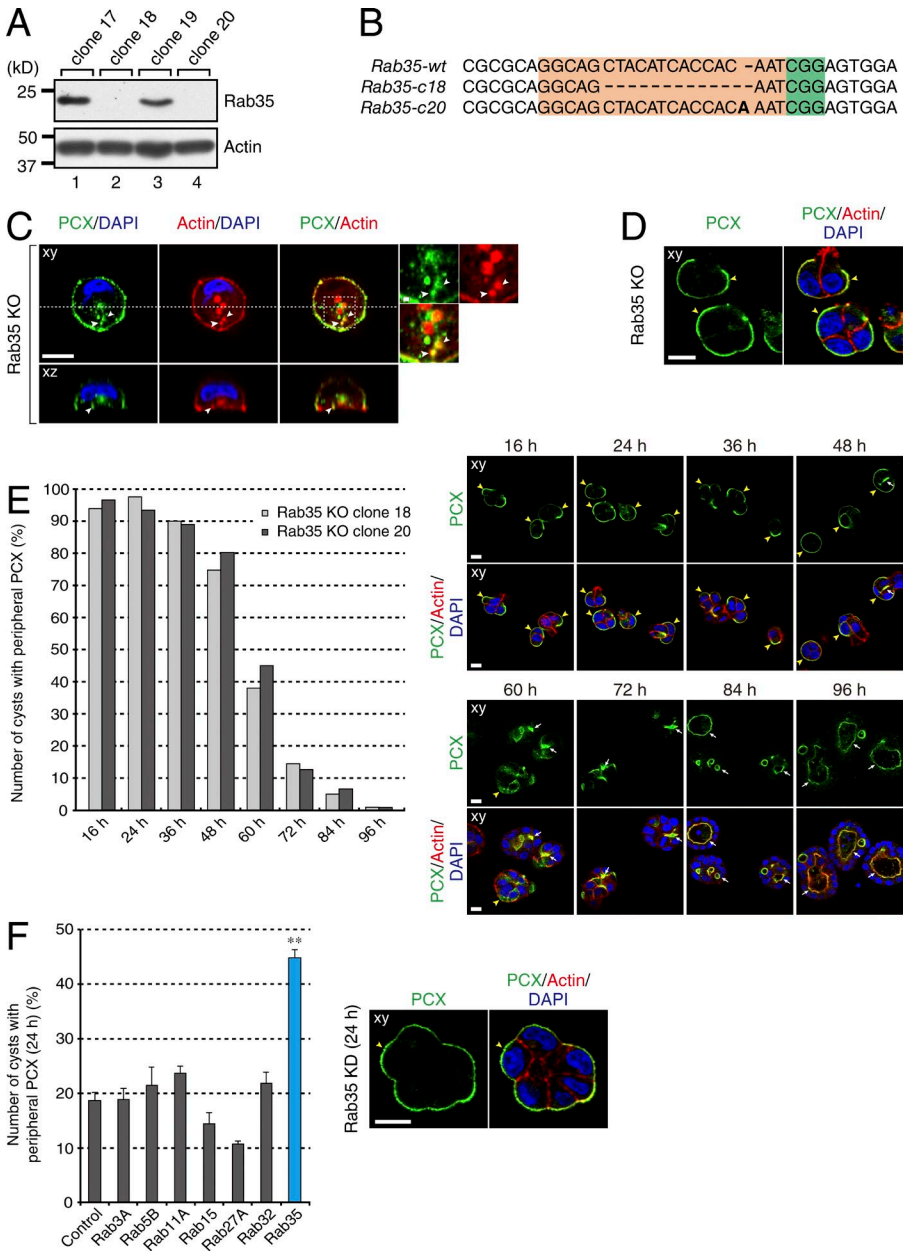

Figure 6. **Characterization of Rab35-KO MDCK II cells.** (A) The *Rab35* gene in MDCK II cells had been specifically disrupted by CRISPR/Cas9 system and the levels of Rab35 protein in selected clones were verified by immunoblotting with specific antibody against Rab35. The KO was successful in clones 18 and 20. (B) Cas9 target sequence against the *Rab35* gene (*Rab35-wt*) and its disruption observed in clones 18 (*Rab35-c18*: 12 nucleotides deletion) and 20 (*Rab35-c20*: one nucleotide insertion). The target and PAM sequences are highlighted in orange and green, respectively. (C and D) Rab35-KO clone 20 cells were plated on glass-bottom dishes (C) or Matrigel-coated glass slides (D) and fixed with PFA 3 h (C) or 24 h (D) after plating. The cells were then stained with anti-PCX antibody (green), Texas red–conjugated phalloidin (red), and DAPI (blue). The arrowheads in C point to PCX dots that localize at actin-rich structures, and the yellow arrowheads in D point to peripheral PCX. (E) Rab35 KO clone 18 or 20 cells were plated on Matrigel-coated glass slides and fixed with PFA at the times indicated. The cells were then stained with anti-PCX antibody, and the cysts with peripheral PCX were counted (left graph). Bars on the graph represent the number of cysts (%) with peripheral PCX scored once for each clone (n > 150). Note that the degree of polarity reversal, which occurs with increased culturing time, is comparable for both clones. The microscopic images on the right side of the graph show representative phenotypes of the clone 20. The white arrows and yellow arrowheads point apical PCX and peripheral PCX, respectively. (F) MDCK II cells that had been treated with indicated *Rab* siRNA, were plated on Matrigel-coated glass slides and fixed with PFA 24 h after plating. The cells were then stained with anti-PCX antibody and the cysts with peripheral PCX were counted. Values represent the mean and SEM of at least three independent experiments (n > 100 in each experiment). Significance was determined by one-way analysis of variance with Dunnett's post-test at 95% confidence interval. **, P < 0.01. The microscopic images on the right side of the graph shows a representative Rab35-KD cyst 24 h after seeding. The yellow arrowhead points peripheral PCX. Bars: 10 µm; (insets) 1 µm.

extent, the reexpression of Rab35(TS/TA) mutant. In contrast, the Rab35(S5A) mutant was unable to rescue the colocalization at all (Fig. 7, D and E). These Rab35 KO-rescue results together with the aforementioned data of Rab35 effectors KD (Fig. 7 A) collectively point at OCRL as the main effector through which Rab35 regulates PCX trafficking in 2D cells, although ACAP2 may also partly contribute to this pathway. It should be noted, however, that KD of OCRL in 3D cysts (24 h) did not induce an inverted phenotype, indicating that a different Rab35 effector should function in PCX trafficking in 3D cysts. Interestingly, in Matrigel culture, only ACAP2 KD induced the inverted phenotype, identical to the one observed in Rab35-KD/KO cysts (Fig. 7 B). In accordance with the ACAP2-KD data, the inverted phenotype of Rab35-KO cells was unable to be rescued by reexpression of either of the ACAP2 binding-deficient mutants, whereas wild-type Rab35 clearly rescued it (Fig. 7 F). Thus, ACAP2 is likely to act as a major Rab35 effector during PCX trafficking in 3D cysts.

Collectively, these results indicate that under 2D and 3D culture conditions, Rab35 differently regulates PCX trafficking by using distinct effector molecules (i.e., OCRL in 2D cells and ACAP2 in 3D cysts), and thereby its depletion leads to distinct phenotypes (i.e., clustered PCX phenotype in 2D cells and inverted phenotype in 3D cells).

Discussion

MDCK II cells are widely used to study protein trafficking in polarizing epithelia and provide a useful simplified model of polarity development in vivo. They create different structures depending on culture conditions: 2D monolayers with a free apical site facing the medium when grown on glass-bottom dishes and 3D cysts with an apical site at the luminal membrane when grown in the Matrigel culture (Fig. 1 C). Both of these structures share characteristic features of polarized epithelia: division of

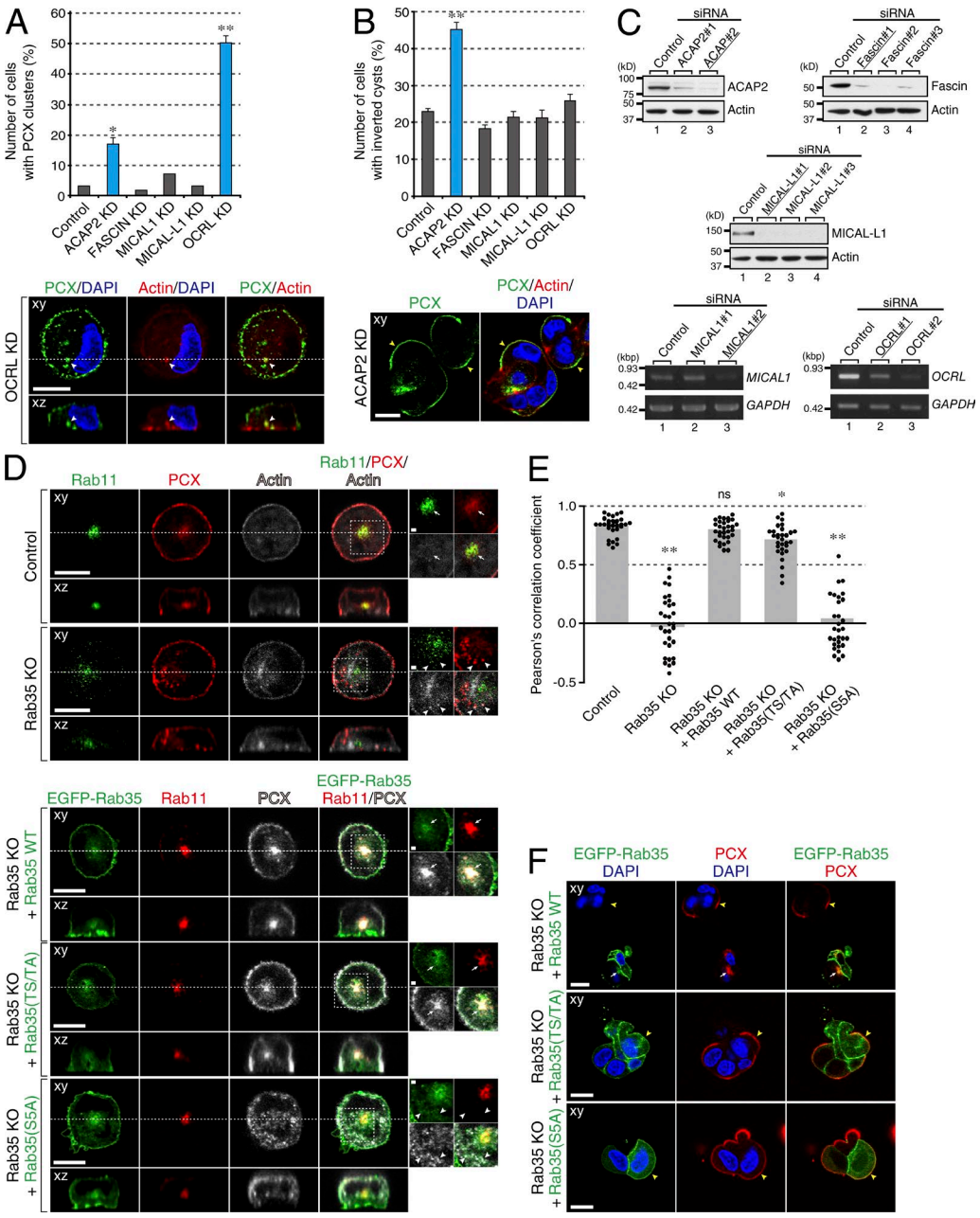

Figure 7. **Rab35 utilizes different effectors in 2D and 3D culture conditions to regulate PCX trafficking.** (A and B) MDCK II cells that had been treated with control siRNA or siRNA against indicated Rab35 effectors were plated on glass-bottom dishes (A) or Matrigel-coated glass slides (B) and fixed with PFA 3 h (A) or 24 h (B) after plating. The cells were then stained with anti-PCX antibody (green), Texas red–conjugated phalloidin (red), and DAPI (blue). Values represent the mean and SEM of at least three independent experiments ($n > 100$ in each experiment). Significance was determined by one-way analysis of variance with Dunnett's post-test at 95% confidence interval. *, $P < 0.05$; **, $P < 0.01$. Bottom images show typical OCRL KD cells (A) and ACAP2 KD cells (B). (C) KD efficiency of siRNAs against Rab35 effectors as revealed by immunoblotting with specific antibody against each effector. siRNAs against ACAP2, Fascin, MIC AL1, MICAL-L1, and OCRL were transfected into MDCK II cells. For ACAP2, Fascin, and MICAL-L1 the level of endogenous protein expression was detected with specific antibodies. For MICAL1 and OCRL the level of gene expression was determined by RT-PCR. Underlined siRNAs were used for the KD experiments. (D) Rab35-KO MDCK II cells were transfected with plasmids carrying EGFP-tagged wild-type (WT) Rab35, a Rab35(TS/TA) mutant with decreased affinity for ACAP2, or a Rab35(S5A) mutant completely unable to bind ACAP2 and with decreased affinity for other Rab35 effectors (Etoh and Fukuda, 2015). Control cells, Rab35-KO cells, and transfected Rab35-KO cells were then plated on glass-bottom dishes and fixed with PFA 3 h after plating. Control and Rab35-KO cells were stained with anti-Rab11 antibody (green), anti-PCX antibody (red) and Alexa Fluor 633 phalloidin (white). The transfected Rab35-KO cells were stained with anti-Rab11 antibody (red) and anti-PCX antibody (white). (E) The graph shows Pearson's correlation coefficient of colocalization between PCX and Rab11 for cells shown in D. PCCs were calculated for at least 30 cells from three independent experiments. Significance was determined by one-way analysis of variance with Dunnett's post-test at 95% confidence interval. *, $P < 0.05$; **, $P < 0.01$; ns, nonsignificant. (F) Rab35-KO MDCK II cells were transfected with plasmids carrying EGFP-tagged Rab35 WT, the Rab35(TS/TA) mutant, or the Rab35(S5A) mutant. The cells were then plated on Matrigel-covered glass slides, fixed with PFA 24 h after plating, and stained with anti-PCX antibody (red) and DAPI (blue). Note that in 2D cells endosomal localization of PCX can be rescued by wild-type Rab35 and to some extent Rab35(TS/TA) mutant, whereas in 3D cysts, the inverted phenotype can only be rescued by wild-type Rab35. The white arrows, white arrowheads, and yellow arrowheads (D and F) point to RE-localized PCX, non-RE intracellular PCX, and peripheral PCX, respectively. For cells growing on Matrigel (B and F), the confocal xy section is shown. For cells growing on glass-bottom dishes (A and D), the confocal xy section (top) and the xz section (bottom), which corresponds to the dashed line in the xy section, are shown. Bars: 10 µm; (insets) 1 µm.

their surface into two functionally distinct membrane domains separated by tight junctions. Transcytosis of PCX from the outer plasma membrane to the newly formed apical membrane is the hallmark of polarity establishment in MDCK II cells. Several regulators of PCX transcytosis have previously been reported (Bryant et al., 2010; Gálvez-Santisteban et al., 2012), but its exact route and mechanism are not completely understood. In the present study, we demonstrated through comprehensive analysis of Rab GTPases that the transcytosis pathway of PCX is differently regulated during MDCK II polarization into 2D monolayer structure and 3D cyst structure and we gave further insight into Rab35 engagement in PCX trafficking under both culture conditions. Although PCX en route to the apical domain traversed the same compartments (i.e., early endosomes and Rab11-positive REs) both under 2D and 3D culture conditions (Figs. 2 and S2), the results of our KD screening of Rab GTPases showed that the regulation of PCX trafficking was markedly different. Even though majority of Rabs were similarly engaged in PCX trafficking under both culture conditions, a significant number turned out to be important only during polarity development in 2D cell culture (Rab13 and Rab14) or only in 3D cell culture (Rab4, Rab15, Rab19, and Rab25; Figs. 4 and 5 and Table 2). Rab35 was found to influence PCX trafficking in both 2D and 3D cell cultures, but the phenotypes resulted from its KD were drastically different under both conditions (actin-rich clusters in 2D cells versus inverted 3D cysts; Fig. 6, C and D). The results of KD of Rab35 effectors further revealed that PCX trafficking was mainly governed by different effectors in 2D (OCRL; Fig. 7, A, D, and E) and 3D (ACAP2; Fig. 7, B and F) cell cultures, even though MDCK II cells express all five Rab35 effectors (Fig. 7 C).

One of the most important findings in this study is that Rab35-KO MDCK II cysts exhibit the inverted phenotype with PCX retained at the peripheral plasma membrane, in contrast to the single-lumen formation in control MDCK II cells, when grown in the Matrigel culture (Fig. 6 D). Such phenotype was not observed at all in cells growing on glass-bottom dishes, in which, even though PCX was trapped in actin-rich clusters en route to the apical surface, it was properly internalized. A similar inverted phenotype has previously been reported in cysts expressing a dominant-negative form of Rac1 (O'Brien et al., 2001), cysts with depleted small GTPase Arf6 (Monteleon et al., 2012), or cysts grown in the presence of function-blocking antibody against β1-integrin (Bryant et al., 2014). All of these proteins are connected with signaling pathway from extracellular matrix to the cell interior, starting from matrix components binding to integrin dimers, which leads to Arf6 and Rac1 activation and further signal transduction (Monteleon et al., 2012; Bryant et al., 2014). Because Rab35, together with Arf6, has previously been reported to regulate β1-integrin trafficking (Allaire et al., 2013), and because ACAP2, whose KD also induced cyst inversion (Fig. 7 B), is a Rab35-associated GTPase-activating protein (GAP) for Arf6 (Jackson et al., 2000; Kanno et al., 2010), it is highly possible that the inverted phenotype observed in Rab35-KO cysts is the consequence of improper β1-integrin recycling, caused by dysregulation of interplay between Rab35, ACAP2, and Arf6. Actually, our unpublished observations of cysts stained with specific anti–β1-integrin antibody showed that even though β1-integrin is abundantly present in the basal membrane of control cysts, it is practically lost from the basal membrane of Rab35-KO cysts (unpublished data). Because PCX KD did not induce an inverted phenotype but rather caused a "no lumen phenotype" (Fig. S1 C), we speculate that the polarity inversion in Rab35-KO cysts is not directly caused by impaired PCX trafficking. In contrast to 3D cysts, however, the Rab35–ACAP2 axis is not involved in polarity development under 2D culture conditions. Instead, Rab35 KO in 2D cells induced formation of actin-rich clusters, a phenotype that was mainly mimicked by OCRL depletion (Fig. 7 A). OCRL is a phosphatidylinositol 5-phosphatase, whose mutations are known to cause oculocerebrorenal syndrome of Lowe, a severe disease that is characterized by renal proximal tubular dysfunction (Attree et al., 1992). It has been shown that OCRL regulates trafficking via early endosomes through its 5-phosphatase activity. Depletion of OCRL in epithelial HK2 cells resulted in ectopic accumulation of its substrate PtdIns(4,5)P_2 at the early endosomal membrane, which in turn triggered N-WASP-dependent increase in endosomal F-actin. Consequently, OCRL depletion caused retention of different proteins passing through early endosomes, including apical glycoprotein megalin (Takeda et al., 2003; Vicinanza et al., 2011; Cauvin et al., 2016). It is thus likely that PCX clustering in actin-rich structures, which we observed in Rab35-KO cells, is in fact caused by its retention in PtdIns(4,5)P_2-enriched early endosomes. OCRL is a Rab effector showing very broad Rab binding specificity and can interact with Rab1, Rab3, Rab5, Rab6, Rab8, Rab13, Rab22B, and Rab35 in vitro (Hyvola et al., 2006; Fukuda et al., 2008). However, out of all these Rabs, excluding Rab1, Rab6, and Rab22B, which did not colocalize with PCX, only Rab35 depletion caused intracellular PCX entrapment like in OCRL-KD cells (Figs. 4 and 7 A), strongly suggesting that Rab35, but not any other OCRL-associated Rab, mediates OCRL-dependent endosomal actin regulation in 2D MDCK II cells.

In summary, this study is the first to demonstrate by the comprehensive analysis of Rab GTPases that the mechanism of PCX trafficking to the apical membrane is markedly different between 2D and 3D cell cultures, although endocytosed PCX is transported to the apical membrane through the same compartments under both culture conditions. We found that in 2D cell culture, Rab35 regulates endosomal PCX trafficking mainly through interaction with OCRL, whereas in 3D cell culture, it regulates uptake of PCX from the outer plasma membrane through specific interaction with ACAP2. Our findings also indicate that the information obtained from 2D cell culture cannot be simply extrapolated to 3D cell culture without additional inquiries. Future investigation of Rab-mediated trafficking of proteins other than PCX will clarify the distinct mechanisms of polarity development in 2D monolayers and 3D cysts.

Materials and methods

Antibodies, plasmids, and siRNAs

Anti-PCX rabbit polyclonal antibody was produced by using purified GST-tagged C-terminal domain of canine PCX (aa residues 501–571; SQRKDQQRLTEELQTVENGYHDNPTLEVMETSS EMQEKKVVNLNGELGDSWIVPLDNLAKDDLDEEEDTHL) as an antigen, and they were affinity-purified with antigen-immobilized beads as described previously (Fukuda and Mikoshiba, 1999). Rabbit polyclonal antibodies against specific Rab isoforms (Rab3A, Rab3B, Rab3C, Rab3D, Rab4A, Rab4B, Rab5A, Rab5B, Rab5C, Rab8A, Rab11A, Rab11B, Rab13, Rab14, Rab15, Rab17, Rab19, Rab20, Rab24, Rab27A, Rab27B, Rab30, Rab32, Rab33A,

Rab34, Rab35, and Rab37) were similarly produced by using purified GST-tagged Rabs (Itoh et al., 2008) as an antigen and affinity purified as described previously (Imai et al., 2004; Saegusa et al., 2006; Tsuboi and Fukuda, 2006; Tamura et al., 2009; Kobayashi and Fukuda, 2012; Mori et al., 2012; Kobayashi et al., 2014; Aizawa and Fukuda, 2015). Anti–E-cadherin rat monoclonal antibody (Takara Bio Inc.), anti-EEA1, anti-GM130, and anti-Rab11 mouse monoclonal antibodies (BD), anti-Rab10 rabbit monoclonal antibody (Cell Signaling Technology), anti-TfR mouse monoclonal antibody (Invitrogen), HRP-conjugated anti-FLAG tag (M2) mouse monoclonal antibody (Sigma-Aldrich), anti–β-actin mouse monoclonal antibody (Applied Biological Materials), anti-ACAP2/centaurin-β2 goat polyclonal antibody (Abcam), anti-Fascin mouse monoclonal antibody (EMD Millipore), and anti–MICAL-L1 mouse polyclonal antibody (Abnova) were obtained commercially.

pEGFP-C1 (Takara Bio Inc.) or pEF-FLAG tag expression vectors carrying cDNAs of mouse Rabs were prepared as described previously (Fukuda, 2003; Matsui et al., 2011). A mutant mouse Rab35(TS/TA) carrying a Thr-to-Ser and Thr-to-Ala double mutation at aa positions 76 and 81, respectively, and Rab35(S5A) carrying a swapping mutation in the switch II region between Rab35 (aa 70–76) and Rab5A (aa 82–88) were also prepared as described previously (Etoh and Fukuda, 2015). The cDNA encoding the C-terminal domain of canine PCX (aa 501–571) was amplified from MDCK II cDNAs by conventional PCR techniques with specific oligonucleotides as described previously (Yasuda et al., 2012) and subcloned into the pGEX-4T-3 vector (GE Healthcare). The canine Rab23 and Rab25 cDNAs were similarly amplified and subcloned into the pEF-BOS expression vector (Fukuda, 2003).

siRNAs used in the main figures are listed in Table S1. Except for Rab12, Rab17, Rab23, and Rab25, siRNAs against mouse Rabs (designated as "M" in Fig. S4; Matsui and Fukuda, 2013) or human Rabs (Aizawa and Fukuda, 2015) were also effective against canine Rabs (Fig. S4). siRNAs against canine Rab12, Rab17, Rab23, and Rab25 were chemically synthesized by Nippon Gene Co.

Cell culture, transfection, and drug treatment

MDCK II cells were precultured in DMEM (Wako Pure Chemical Industries) containing 10% fetal bovine serum, penicillin G (100 U/ml), and streptomycin (100 µg/ml) before being replated for subsequent plasmid or siRNA transfection or drug treatment. Plasmids and siRNAs were transfected into MDCK II cells by using Lipofectamine 2000 and Lipofectamine RNAiMAX (Invitrogen), respectively, each according to the manufacturer's protocol. 16 h after plasmid transfection or 48 h after siRNA transfection, cells were replated for subsequent microscopic observations. For 2D cell culture observations, the cells were trypsinized to a single-cell suspension, plated on uncoated glass-bottom dishes (35-mm dish; MatTek), and cultured in DMEM. For 3D cysts, the cells were trypsinized, plated on glass slides coated with Matrigel (Growth Factor Reduced; BD), and cultured in DMEM medium with 2% Matrigel.

Immunofluorescence analysis

Immunostaining of MDCK II 2D monolayers and 3D cysts was performed as described previously (Yasuda et al., 2015). In brief, cells were fixed with 4% PFA for 10 min (2D) or 30 min (3D) at room temperature, permeabilized with 0.3% Triton X-100 in PBS for 2 min (2D) or 30 min (3D), and blocked with the blocking buffer (1% BSA and 0.1% Triton X-100 in PBS) for 30 min at room temperature. The cells were then incubated for 2 h at room temperature (2D) or overnight at 4°C (3D) in the same buffer containing primary antibodies at the following concentrations: anti-PCX antibody, 0.5 µg/ml; anti-EEA1 antibody, 1/100 dilution; anti-GM130 antibody, 1/100 dilution; anti-Rab11 antibody, 1/100 dilution; and anti-TfR antibody, 1/100 dilution. After that, cells were incubated with secondary antibodies (Alexa Fluor 488 or 594 conjugated; Invitrogen) and DAPI. To visualize actin, cells were stained with Texas red–conjugated phalloidin (1/200 dilution; Invitrogen). The stained cells were examined for immunofluorescence signals at room temperature with a confocal fluorescence microscope (FluoView 1000; Olympus) through an objective lens (100× magnification, NA 1.45; Olympus) and an EM-CCD camera (C9100; Hamamatsu Photonics) and with FluoView software (version 2.1c; Olympus).

Immunoblot analysis

MDCK II cells (2×10^5 cells/3.5-cm dish) were cultured for 48 h, harvested, and lysed in the lysis buffer (50 mM Hepes-KOH, pH 7.2, 150 mM NaCl, 1 mM $MgCl_2$, 1% Triton X-100, and protease inhibitor cocktail; Roche). Proteins were separated by 10% SDS-PAGE, transferred to a nitrocellulose membrane, and incubated overnight with specific primary antibodies at 4°C. The blots were subsequently incubated for 1 h at room temperature with appropriate HRP-conjugated secondary antibodies, and immunoreactive bands were detected by chemiluminescence.

RNA isolation and RT-PCR analysis

Total RNA was isolated from MDCK II cells by lysing the cells with TRI Reagent (Sigma-Aldrich), followed by chloroform extraction and 2-propanol precipitation. The isolated total RNA was subjected to reverse transcription using the ReverTra Ace -Plus- RT-PCR kit (Toyobo) to synthesize cDNAs. Specific oligonucleotides for canine MICAL1, OCRL, and Rab12 were designed to amplify fragments of 620, 711, and 445 bp, respectively, from the cDNA obtained: MICAL1 forward primer, 5′-CTGCTCTTGTTGAAAGTGGTGTTACTGCTC-3′; MICAL1 reverse primer, 5′-CTCGTGAAGTCGAAAGCAGAGATG TCA-3′; OCRL forward primer, 5′-GGATCCATGGAGCCGCCGCTC TCGGTTGGA-3′; OCRL reverse primer, 5′-GGATCCGACATACTC TTTCTCTCGCTTTGC-3′; Rab12 forward primer, 5′-ACACAGCAG GTCAGGAGAGATTCAA-3′; and Rab12 reverse primer, 5′-TTAACA GCATCGAACGTGTGGTCTTGGTG-3′. Canine GAPDH was amplified using mouse G3PDH-5′ and G3PDH-3′ primers (BD) as a reference. The cDNA fragments were amplified by PCR using ExTaq DNA polymerase (Takara Bio Inc.) with 30 (for MICAL1), 35 (for OCRL), or 20 (for GAPDH) cycles of denaturation at 94°C for 1 min; annealing at 59°C (for MICAL1), 65°C (for OCRL), or 55°C (for GAPDH) for 2 min; and extension at 72°C for 1 min. PCR products were analyzed by agarose gel electrophoresis.

CRISPR/Cas9 gene KO

Guide RNA for Rab35 knockout in MDCK II cells was designed using CRISPR Direct webpage (http://crispr.dbcls.jp/) and two corresponding oligonucleotides were synthesized: Rab35-KO sgRNA sense sequence (5′-CACCGGGCAGCTACATCACCACAAT-3′) and Rab35-KO sgRNA antisense sequence (5′-AAACATTGTGGTGAT GTAGCTGCCC-3′). The CRISPR/Cas9-mediated Rab35 KO was performed according to the protocol by Ran et al. (2013). In brief, the sgRNA expression construct was prepared by cloning annealed sgRNA into linearized pSpCas9(BB)-2A-Puro vector (Addgene). The obtained pSpCas9-Rab35KO plasmid was transfected into MDCK II cells, and after 24 h, puromycin (EMD Millipore) was added to the culture medium for selection of transfected cells. Puromycin was removed after another 24 h, and the cells were trypsinized and seeded at 100 cells per 10-cm dish. The remaining cell suspension was used for genotyping through a SURVEYOR assay to gauge overall modification efficiency. The plated cells were allowed to expand for 1 wk until the colonies were formed. Clonal lines were isolated and analyzed through immunoblotting with specific anti-Rab35 antibody to detect

their Rab35 protein level. From the cell lines that showed no Rab35 protein expression on immunoblots, genomic DNA was extracted for sequencing. The cells were lysed with the digestion buffer (100 mM NaCl, 10 mM Tris, pH 8.0, 25 mM EDTA, pH 8.0, 0.5% SDS, and 100 µg/ml proteinase K; Merck) at 50°C overnight to release the genomic DNA into the solution. DNA was extracted with an equal volume of phenol and chloroform, precipitated with ethanol, dried, and diluted in TE (10 mM Tris, pH 8.0, and 1 mM EDTA). 100 ng of the isolated genomic DNA was used for PCR amplification of potentially modified genome fragment (forward primer, 5′-CTACCTCATCACCTCCTC CTCTCACACAAC-3′; reverse primer, 5′-GACCTTGTCTTTCTT GCTCAGGACTGTGTC-3′; 35 cycles of denaturation at 94°C for 30 s, annealing at 65°C for 30 s, and extension at 72°C for 1 min). The PCR product was inserted into the pGEM-T-Easy vector (Promega) and sequenced to detect the modification of the sgRNA target site. The SURVEYOR assay was performed as described in Ran et al. (2013). In brief, the genomic DNA was isolated from the cells and subjected to PCR under the same conditions used for sequencing of the genomic *Rab35* fragment. The amplified fragment was hybridized by heating at 94°C and gradually decreasing the temperature to 25°C. Hybridized product was digested using the SURVEYOR Mutation Detection kit (Transgenomic) and analyzed through agarose gel electrophoresis to detect if digestion occurred, which indicated successful genome disruption by Cas9 endonuclease.

Statistical analysis

The data are presented as means and SEM. Statistical significance was determined using GraphPad Prism software (version 4.0) by one-way analysis of variance with Dunnett's post-test. A probability level of $P < 0.05$ was considered statistically significant.

Online supplemental material

Fig. S1 shows the specificity of anti-PCX antibody and morphology of PCX-KD cells. Fig. S2 shows the colocalization between PCX and organelle markers in 2D and 3D MDCK II cells. Fig. S3 shows the colocalization between endogenous PCX and EGFP-Rabs in 2D MDCK II cells. Fig. S4 shows the effect of KD of Rabs on localization of endogenous PCX in 2D MDCK II cells. Fig. S5 shows the effect of KD of Rabs on single-lumen formation in 3D MDCK II cells. Table S1 lists the siRNA sequences used in this study. Online supplemental material is available at http://www.jcb.org/cgi/content/full/jcb.201512024/DC1. Full images of Figs. S2, S3, and S4 are available in the JCB DataViewer at http://dx.doi.org/10.1083/jcb.201512024.dv.

Acknowledgments

We thank Takao Yasuda for help in the initial screening for Rabs and for generation of the anti-PCX antibody, Yuta Homma for help in the establishment of Rab35-KO clones, Megumi Aizawa for technical assistance, and members of the Fukuda Laboratory for valuable discussions.

This work was supported in part by Grants-in-Aid for Scientific Research from the Ministry of Education, Culture, Sports, and Technology (MEXT) of Japan (grants 15H04367 and 15H01198 to M. Fukuda) and by a grant from the Naito Foundation (to M. Fukuda). P.S. Mrozowska was supported by the Japanese Government (MEXT) Scholarship.

The authors declare no competing financial interests.

Submitted: 7 December 2015
Accepted: 18 March 2016

Note added in proof. Klinkert et al. (2016. *Nat. Commun.* http://dx.doi.org/10.1038/ncomms11166) recently reported that Rab35 directly interacts with the cytoplasmic tail of podocalyxin and acts as a molecular tether that captures vesicles containing key apical determinants at the first cleavage site of MDCK cells. Consequently, Rab35 inactivation leads to complete inversion of apicobasal polarity in 3D cysts.

References

Aizawa, M., and M. Fukuda. 2015. Small GTPase Rab2B and its specific binding protein Golgi-associated Rab2B interactor-like 4 (GARI-L4) regulate Golgi morphology. *J. Biol. Chem.* 290:22250–22261. http://dx.doi.org/10.1074/jbc.M115.669242

Allaire, P.D., M. Seyed Sadr, M. Chaineau, E. Seyed Sadr, S. Konefal, M. Fotouhi, D. Maret, B. Ritter, R.F. Del Maestro, and P.S. McPherson. 2013. Interplay between Rab35 and Arf6 controls cargo recycling to coordinate cell adhesion and migration. *J. Cell Sci.* 126:722–731. http://dx.doi.org/10.1242/jcs.112375

Attree, O., I.M. Olivos, I. Okabe, L.C. Bailey, D.L. Nelson, R.A. Lewis, R.R. McInnes, and R.L. Nussbaum. 1992. The Lowe's oculocerebrorenal syndrome gene encodes a protein highly homologous to inositol polyphosphate-5-phosphatase. *Nature.* 358:239–242. http://dx.doi.org/10.1038/358239a0

Bryant, D.M., A. Datta, A.E. Rodríguez-Fraticelli, J. Peränen, F. Martín-Belmonte, and K.E. Mostov. 2010. A molecular network for *de novo* generation of the apical surface and lumen. *Nat. Cell Biol.* 12:1035–1045. http://dx.doi.org/10.1038/ncb2106

Bryant, D.M., J. Roignot, A. Datta, A.W. Overeem, M. Kim, W. Yu, X. Peng, D.J. Eastburn, A.J. Ewald, Z. Werb, and K.E. Mostov. 2014. A molecular switch for the orientation of epithelial cell polarization. *Dev. Cell.* 31:171–187. http://dx.doi.org/10.1016/j.devcel.2014.08.027

Casanova, J.E., X. Wang, R. Kumar, S.G. Bhartur, J. Navarre, J.E. Woodrum, Y. Altschuler, G.S. Ray, and J.R. Goldenring. 1999. Association of Rab25 and Rab11a with the apical recycling system of polarized Madin-Darby canine kidney cells. *Mol. Biol. Cell.* 10:47–61. http://dx.doi.org/10.1091/mbc.10.1.47

Cauvin, C., M. Rosendale, N. Gupta-Rossi, M. Rocancourt, P. Larraufie, R. Salomon, D. Perrais, and A. Echard. 2016. Rab35 GTPase triggers switch-like recruitment of the Lowe syndrome lipid phosphatase OCRL on newborn endosomes. *Curr. Biol.* 26:120–128. http://dx.doi.org/10.1016/j.cub.2015.11.040

Cong, L., F.A. Ran, D. Cox, S. Lin, R. Barretto, N. Habib, P.D. Hsu, X. Wu, W. Jiang, L.A. Marraffini, and F. Zhang. 2013. Multiplex genome engineering using CRISPR/Cas systems. *Science.* 339:819–823. http://dx.doi.org/10.1126/science.1231143

Dambournet, D., M. Machicoane, L. Chesneau, M. Sachse, M. Rocancourt, A. El Marjou, E. Formstecher, R. Salomon, B. Goud, and A. Echard. 2011. Rab35 GTPase and OCRL phosphatase remodel lipids and F-actin for successful cytokinesis. *Nat. Cell Biol.* 13:981–988. http://dx.doi.org/10.1038/ncb2279

Doyonnas, R., D.B. Kershaw, C. Duhme, H. Merkens, S. Chelliah, T. Graf, and K.M. McNagny. 2001. Anuria, omphalocele, and perinatal lethality in mice lacking the CD34-related protein podocalyxin. *J. Exp. Med.* 194:13–27. http://dx.doi.org/10.1084/jem.194.1.13

Etoh, K., and M. Fukuda. 2015. Structure-function analyses of the small GTPase Rab35 and its effector protein centaurin-β2/ACAP2 during neurite outgrowth of PC12 cells. *J. Biol. Chem.* 290:9064–9074. http://dx.doi.org/10.1074/jbc.M114.611301

Fukuda, M. 2003. Distinct Rab binding specificity of Rim1, Rim2, rabphilin, and Noc2: identification of a critical determinant of Rab3A/Rab27A recognition by Rim2. *J. Biol. Chem.* 278:15373–15380. http://dx.doi.org/10.1074/jbc.M212341200

Fukuda, M. 2008. Regulation of secretory vesicle traffic by Rab small GTPases. *Cell. Mol. Life Sci.* 65:2801–2813. http://dx.doi.org/10.1007/s00018-008-8351-4

Fukuda, M., and K. Mikoshiba. 1999. A novel alternatively spliced variant of synaptotagmin VI lacking a transmembrane domain: implications for distinct functions of the two isoforms. *J. Biol. Chem.* 274:31428–31434. http://dx.doi.org/10.1074/jbc.274.44.31428

Fukuda, M., E. Kanno, K. Ishibashi, and T. Itoh. 2008. Large scale screening for novel Rab effectors reveals unexpected broad Rab binding specificity. *Mol. Cell. Proteomics.* 7:1031–1042. http://dx.doi.org/10.1074/mcp.M700569-MCP200

Gálvez-Santisteban, M., A.E. Rodriguez-Fraticelli, D.M. Bryant, S. Vergarajauregui, T. Yasuda, I. Bañón-Rodríguez, I. Bernascone,

A. Datta, N. Spivak, K. Young, et al. 2012. Synaptotagmin-like proteins control the formation of a single apical membrane domain in epithelial cells. *Nat. Cell Biol.* 14:838–849. http://dx.doi.org/10.1038/ncb2541

Hutagalung, A.H., and P.J. Novick. 2011. Role of Rab GTPases in membrane traffic and cell physiology. *Physiol. Rev.* 91:119–149. http://dx.doi.org/10.1152/physrev.00059.2009

Hyvola, N., A. Diao, E. McKenzie, A. Skippen, S. Cockcroft, and M. Lowe. 2006. Membrane targeting and activation of the Lowe syndrome protein OCRL1 by rab GTPases. *EMBO J.* 25:3750–3761. http://dx.doi.org/10.1038/sj.emboj.7601274

Imai, A., S. Yoshie, T. Nashida, H. Shimomura, and M. Fukuda. 2004. The small GTPase Rab27B regulates amylase release from rat parotid acinar cells. *J. Cell Sci.* 117:1945–1953. http://dx.doi.org/10.1242/jcs.01048

Itoh, T., N. Fujita, E. Kanno, A. Yamamoto, T. Yoshimori, and M. Fukuda. 2008. Golgi-resident small GTPase Rab33B interacts with Atg16L and modulates autophagosome formation. *Mol. Biol. Cell.* 19:2916–2925. http://dx.doi.org/10.1091/mbc.E07-12-1231

Jackson, T.R., F.D. Brown, Z. Nie, K. Miura, L. Foroni, J. Sun, V.W. Hsu, J.G. Donaldson, and P.A. Randazzo. 2000. ACAPs are Arf6 GTPase-activating proteins that function in the cell periphery. *J. Cell Biol.* 151:627–638. http://dx.doi.org/10.1083/jcb.151.3.627

Kanno, E., K. Ishibashi, H. Kobayashi, T. Matsui, N. Ohbayashi, and M. Fukuda. 2010. Comprehensive screening for novel Rab-binding proteins by GST pull-down assay using 60 different mammalian Rabs. *Traffic.* 11:491–507. http://dx.doi.org/10.1111/j.1600-0854.2010.01038.x

Kerjaschki, D., D.J. Sharkey, and M.G. Farquhar. 1984. Identification and characterization of podocalyxin--the major sialoprotein of the renal glomerular epithelial cell. *J. Cell Biol.* 98:1591–1596. http://dx.doi.org/10.1083/jcb.98.4.1591

Kobayashi, H., and M. Fukuda. 2012. Rab35 regulates Arf6 activity through centaurin-β2 (ACAP2) during neurite outgrowth. *J. Cell Sci.* 125:2235–2243. http://dx.doi.org/10.1242/jcs.098657

Kobayashi, H., and M. Fukuda. 2013a. Rab35 establishes the EHD1-association site by coordinating two distinct effectors during neurite outgrowth. *J. Cell Sci.* 126:2424–2435. http://dx.doi.org/10.1242/jcs.117846

Kobayashi, H., and M. Fukuda. 2013b. Arf6, Rab11 and transferrin receptor define distinct populations of recycling endosomes. *Commun. Integr. Biol.* 6:e25036. http://dx.doi.org/10.4161/cib.25036

Kobayashi, H., K. Etoh, N. Ohbayashi, and M. Fukuda. 2014. Rab35 promotes the recruitment of Rab8, Rab13 and Rab36 to recycling endosomes through MICAL-L1 during neurite outgrowth. *Biol. Open.* 3:803–814. http://dx.doi.org/10.1242/bio.20148771

Martin-Belmonte, F., and K. Mostov. 2008. Regulation of cell polarity during epithelial morphogenesis. *Curr. Opin. Cell Biol.* 20:227–234. http://dx.doi.org/10.1016/j.ceb.2008.01.001

Martin-Belmonte, F., A. Gassama, A. Datta, W. Yu, U. Rescher, V. Gerke, and K. Mostov. 2007. PTEN-mediated apical segregation of phosphoinositides controls epithelial morphogenesis through Cdc42. *Cell.* 128:383–397. http://dx.doi.org/10.1016/j.cell.2006.11.051

Matsui, T., and M. Fukuda. 2013. Rab12 regulates mTORC1 activity and autophagy through controlling the degradation of amino-acid transporter PAT4. *EMBO Rep.* 14:450–457. http://dx.doi.org/10.1038/embor.2013.32

Matsui, T., T. Itoh, and M. Fukuda. 2011. Small GTPase Rab12 regulates constitutive degradation of transferrin receptor. *Traffic.* 12:1432–1443. http://dx.doi.org/10.1111/j.1600-0854.2011.01240.x

Meder, D., A. Shevchenko, K. Simons, and J. Füllekrug. 2005. Gp135/podocalyxin and NHERF-2 participate in the formation of a preapical domain during polarization of MDCK cells. *J. Cell Biol.* 168:303–313. http://dx.doi.org/10.1083/jcb.200407072

Monteleon, C.L., A. Sedgwick, A. Hartsell, M. Dai, C. Whittington, S. Voytik-Harbin, and C. D'Souza-Schorey. 2012. Establishing epithelial glandular polarity: interlinked roles for ARF6, Rac1, and the matrix microenvironment. *Mol. Biol. Cell.* 23:4495–4505. http://dx.doi.org/10.1091/mbc.E12-03-0246

Mori, Y., T. Matsui, Y. Furutani, Y. Yoshihara, and M. Fukuda. 2012. Small GTPase Rab17 regulates dendritic morphogenesis and postsynaptic development of hippocampal neurons. *J. Biol. Chem.* 287:8963–8973. http://dx.doi.org/10.1074/jbc.M111.314385

O'Brien, L.E., T.S. Jou, A.L. Pollack, Q. Zhang, S.H. Hansen, P. Yurchenco, and K.E. Mostov. 2001. Rac1 orientates epithelial apical polarity through effects on basolateral laminin assembly. *Nat. Cell Biol.* 3:831–838. http://dx.doi.org/10.1038/ncb0901-831

Ojakian, G.K., and R. Schwimmer. 1988. The polarized distribution of an apical cell surface glycoprotein is maintained by interactions with the cytoskeleton of Madin-Darby canine kidney cells. *J. Cell Biol.* 107:2377–2387. http://dx.doi.org/10.1083/jcb.107.6.2377

Rahajeng, J., S.S. Giridharan, B. Cai, N. Naslavsky, and S. Caplan. 2012. MICAL-L1 is a tubular endosomal membrane hub that connects Rab35 and Arf6 with Rab8a. *Traffic.* 13:82–93. http://dx.doi.org/10.1111/j.1600-0854.2011.01294.x

Ran, F.A., P.D. Hsu, J. Wright, V. Agarwala, D.A. Scott, and F. Zhang. 2013. Genome engineering using the CRISPR-Cas9 system. *Nat. Protoc.* 8:2281–2308. http://dx.doi.org/10.1038/nprot.2013.143

Saegusa, C., T. Tanaka, S. Tani, S. Itohara, K. Mikoshiba, and M. Fukuda. 2006. Decreased basal mucus secretion by Slp2-a-deficient gastric surface mucous cells. *Genes Cells.* 11:623–631. http://dx.doi.org/10.1111/j.1365-2443.2006.00964.x

Simmons, N.L. 1982. Cultured monolayers of MDCK cells: a novel model system for the study of epithelial development and function. *Gen. Pharmacol.* 13:287–291. http://dx.doi.org/10.1016/0306-3623(82)90047-7

Stenmark, H. 2009. Rab GTPases as coordinators of vesicle traffic. *Nat. Rev. Mol. Cell Biol.* 10:513–525. http://dx.doi.org/10.1038/nrm2728

Stoops, E.H., and M.J. Caplan. 2014. Trafficking to the apical and basolateral membranes in polarized epithelial cells. *J. Am. Soc. Nephrol.* 25:1375–1386. http://dx.doi.org/10.1681/ASN.2013080883

Takeda, T., H. Yamazaki, and M.G. Farquhar. 2003. Identification of an apical sorting determinant in the cytoplasmic tail of megalin. *Am. J. Physiol. Cell Physiol.* 284:C1105–C1113. http://dx.doi.org/10.1152/ajpcell.00514.2002

Tamura, K., N. Ohbayashi, Y. Maruta, E. Kanno, T. Itoh, and M. Fukuda. 2009. Varp is a novel Rab32/38-binding protein that regulates Tyrp1 trafficking in melanocytes. *Mol. Biol. Cell.* 20:2900–2908. http://dx.doi.org/10.1091/mbc.E08-12-1161

Tsuboi, T., and M. Fukuda. 2006. Rab3A and Rab27A cooperatively regulate the docking step of dense-core vesicle exocytosis in PC12 cells. *J. Cell Sci.* 119:2196–2203. http://dx.doi.org/10.1242/jcs.02962

Vicinanza, M., A. Di Campli, E. Polishchuk, M. Santoro, G. Di Tullio, A. Godi, E. Levtchenko, M.G. De Leo, R. Polishchuk, L. Sandoval, et al. 2011. OCRL controls trafficking through early endosomes via PtdIns4,5P_2-dependent regulation of endosomal actin. *EMBO J.* 30:4970–4985. http://dx.doi.org/10.1038/emboj.2011.354

Yasuda, T., C. Saegusa, S. Kamakura, H. Sumimoto, and M. Fukuda. 2012. Rab27 effector Slp2-a transports the apical signaling molecule podocalyxin to the apical surface of MDCK II cells and regulates claudin-2 expression. *Mol. Biol. Cell.* 23:3229–3239. http://dx.doi.org/10.1091/mbc.E12-02-0104

Yasuda, T., P.S. Mrozowska, and M. Fukuda. 2015. Functional analysis of Rab27A and its effector Slp2-a in renal epithelial cells. *Methods Mol. Biol.* 1298:127–139. http://dx.doi.org/10.1007/978-1-4939-2569-8_11

Zhang, J., M. Fonovic, K. Suyama, M. Bogyo, and M.P. Scott. 2009. Rab35 controls actin bundling by recruiting fascin as an effector protein. *Science.* 325:1250–1254. http://dx.doi.org/10.1126/science.1174921

Zhen, Y., and H. Stenmark. 2015. Cellular functions of Rab GTPases at a glance. *J. Cell Sci.* 128:3171–3176. http://dx.doi.org/10.1242/jcs.166074